AGU PUBLICATIONS

Tectonics

RESEARCH ARTICLE
10.1002/2014TC003614

Key Points:
- Extended landward vergent structural zone from the Sunda Trench landward
- Edge of seaward dipping backstop beneath prism crest, coincident vergence change
- Strong inner wedge (suggested lithified sediments) causes enhanced tsunamigenic potential

Supporting Information:
- Supporting Information S1
- Figure S1
- Figure S2
- Figure S3
- Figure S4
- Figure S5
- Figure S6
- Figure S7

Correspondence to:
M. C. G. Frederik,
marina.frederik@utexas.edu

Citation:
Frederik, M. C. G., S. P. S. Gulick, J. A. Austin Jr., N. L. B. Bangs, and Udrekh (2015), What 2-D multichannel seismic and multibeam bathymetric data tell us about the North Sumatra wedge structure and coseismic response, *Tectonics*, *34*, 1910–1926, doi:10.1002/2014TC003614.

Received 16 APR 2014
Accepted 23 AUG 2015
Accepted article online 26 AUG 2015
Published online 25 SEP 2015

What 2-D multichannel seismic and multibeam bathymetric data tell us about the North Sumatra wedge structure and coseismic response

M. C. G. Frederik[1,2], S. P. S. Gulick[1], J. A. Austin Jr.[1], N. L. B. Bangs[1], and Udrekh[2]

[1]University of Texas Institute for Geophysics, John A. and Katherine G. Jackson School of Geosciences, The University of Texas at Austin, Austin, Texas, USA, [2]Badan Pengkajian dan Penerapan Teknologi, Jakarta, Indonesia

Abstract Recent large earthquakes have prompted studies to reevaluate seismicity and rupture propagation behavior along the world's major subduction margins. Our study area covers the entire fore arc from northwest of northern Sumatra to west of Simeulue Island, the southern portion of the 2004 tsunamigenic earthquake rupture zone. The accretionary prism width is up to ~180 km, water depths between ~4.5 km near the Sunda Trench and <1 km on fore-arc high. The wedge consists of a steep outer slope (5–12°), a plateau ~100–120 km wide with anticlinal folds spaced 2–15 km apart, and a steep inner slope adjacent to the Aceh Basin. Analysis of seismic profiles and bathymetry reveal three main structural zones consistent along-strike, from the trench landward: (1) predominantly landward vergent folds, (2) mixed vergent folds, and (3) predominantly seaward vergent folds. This paper uses those zones to propose a geometry of an underlying rigid backstop. This backstop is seaward dipping and extends from under the Aceh Basin to beneath the mixed vergence zone. A dynamic backstop possibly exists seaward of the rigid backstop and is responsible for the steep slope of the outer prism. Indurated accreted sediments form the landward vergence zone. Along with the possible dynamic backstop beneath the outer wedge, and the rigid backstop in the inner wedge, all behave as a solid block coseismically. This block allows great earthquake rupture to propagate farther seaward toward the Sunda Trench, with resultant hazardous tsunamigenic potential.

1. Introduction

Most major earthquakes occur along subduction zones and are capable of producing devastating effects, such as tsunamis, as demonstrated by the 2011 Tohoku (~M_w 9.0) and the 2004 Sumatra-Andaman (~M_w 9.1) events. For these great earthquakes, studies show that seismogenic rupture may have extended close to the trench, likely contributing to the associated large tsunamis. For example, using bathymetric differences recorded between 1999 and 2011, *Fujiwara et al.* [2011] have observed the location of maximum slip for the Tohoku event to be at the Japan Trench, in agreement with slip model [*Pollitz et al.*, 2011]. For northern Sumatra, slip distribution models [*Ammon et al.*, 2005; *Rhie et al.*, 2007] have suggested that the displacement also extended toward the Sunda Trench. Therefore, understanding the geophysically observable morphology and structure of an accretionary prism, such as that near the rupture zone of the 2004 Aceh-Andaman event, should help us understand updip rupture propagation during great earthquakes.

Off western Sumatra, the Indian and Australian Plates are subducting under the Sunda Block (Figure 1). For northern Sumatra, the rate of convergence is 50–55 mm/yr [*Prawirodirdjo et al.*, 2000; *McNeill and Henstock*, 2014]. Subduction started with northward movement of the Indian Plate ~100 Ma [*Sclater and Fisher*, 1974; *Molnar and Tapponnier*, 1975]. Influx of Bengal and related Nicobar Fan sediments started during the late Miocene-Pliocene [*Curray and Moore*, 1971]; accretionary wedge formation offshore Sumatra began in the late Miocene [*Curray and Moore*, 1974]. The major source of sediment forming the accretionary prism offshore of northern Sumatra is the Nicobar Fan. However, since late Pliocene or Pleistocene, the availability of Nicobar Fan sediments may have been restricted by the Ninetyeast Ridge topographic barrier [*Karig et al.*, 1979].

On 26 December 2004, a magnitude ~9.1 earthquake occurred offshore northern Sumatra; its rupture zone extended along a major portion of the subduction zone from Sumatra (Figure 1) to the Andaman Islands [*Ammon et al.*, 2005; *Ishii et al.*, 2005; *Rhie et al.*, 2007]. This great earthquake produced a large tsunami that affected countries neighboring the Indian Ocean and killed over 200,000 people [*Sibuet et al.*, 2007; *Graindorge et al.*, 2008]. Rupture began at a depth of ~50 km and covered an area of ~1250 × 150 km

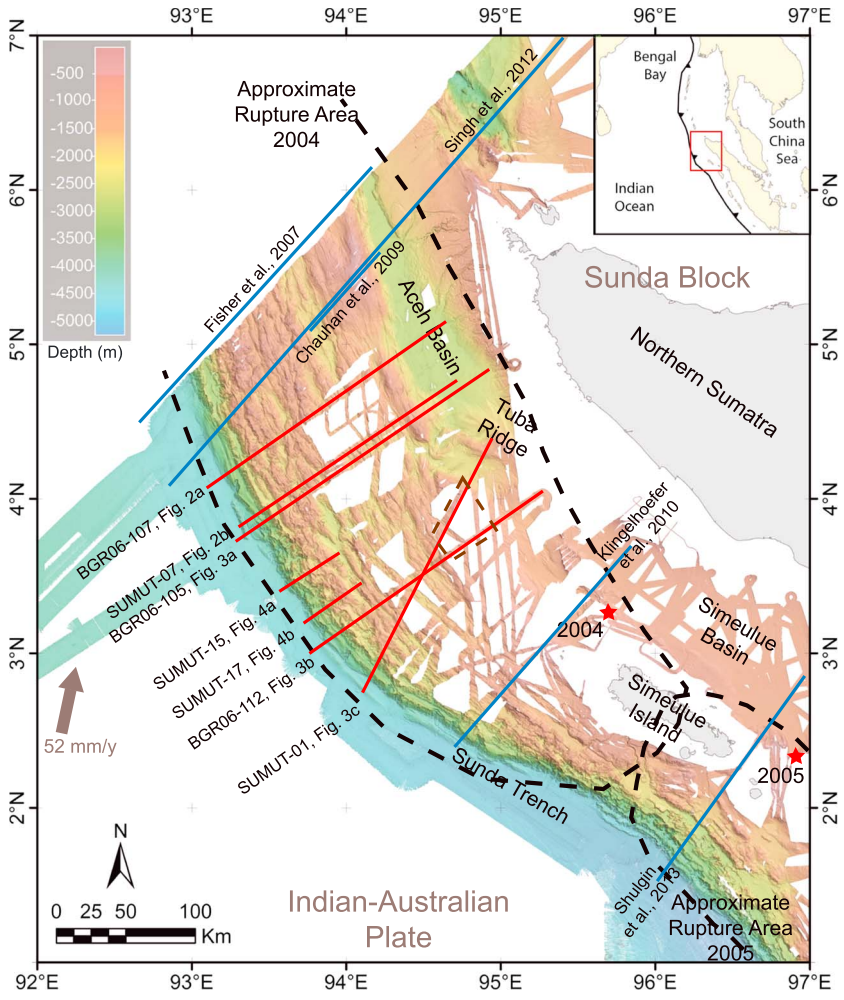

Figure 1. Bathymetric and seismic coverage used for this investigation. MCS (red) tracklines superimposed on bathymetric data merged from various sources (Table 1). The color bar indicates seafloor depths in meters. The bathymetric data show the complex surficial structural fabric of the accretionary wedge. The red stars denote epicenters of 2004 and 2005 great earthquakes, and the black dashed lines show associated rupture areas [*Briggs et al.*, 2006]. The brown dashed trapezium shows region of topographical high (Figures 3b and 3c). Our structural analysis focuses on seven MCS profiles (red lines), labeled from north to south: BGR06-107, SUMUT-07, BGR06-105, SUMUT-15, SUMUT-17, BGR06-112, and SUMUT-01. The blue lines are seismic profile studies published by indicated authors. See the text for details.

(187,500 km^2) [*Ammon et al.*, 2005; *Ishii et al.*, 2005; *Banerjee et al.*, 2007; *Rhie et al.*, 2007]. Three months later, in March 2005, another great earthquake (~M_w 8.7, rupture area ~40,000 km^2) occurred south of the epicenter of the 2004 rupture [*Banerjee et al.*, 2007]. This earthquake did not produce a large tsunami [*Geist et al.*, 2006].

This paper extends our knowledge of the structure and morphology of the accretionary wedge offshore of northern Sumatra, using 2-D multichannel seismic (MCS) profiles and a synthesis of multibeam bathymetric data. These results lead us to propose a new geometry of a rigid backstop forming the core of this part of the accretionary wedge, with implications for its seismogenic behavior.

2. Study Area and Previous Work

Our study area, between 1–7°N and 92–97°E, extends over the entire fore arc, from northwest of northern Sumatra to west of Simeulue Island (Figure 1). The accretionary wedge within our study area is up to ~180 km wide [*Fisher et al.*, 2007]; seafloor depths are ranging from ~4.5 km near the Sunda Trench [*Gulick et al.*, 2011] to <1 km on the fore-arc high proximal to the Aceh (fore-arc) Basin. The wedge narrows to

~125 km southward around Simeulue Island. This accretionary prism is characterized by complex structures, including both seaward and landward vergent thrust zones and piggyback basins with growth strata [*Karig*, 1977; *Henstock et al*., 2006; *Sibuet et al*., 2007; *Graindorge et al*., 2008].

Landward vergence of folded sediments in subduction zones is not generally observed, although such vergence occurs in the Cascadia, southwest Alaska, southwest Japan, and northern Panama convergent margins [*Moore and Allwardt*, 1980; *Byrne and Hibbard*, 1987; *Reed et al*., 1990; *MacKay et al*., 1992; *Gulick et al*., 1998]. Landward vergent structures may form as a result of a seaward dipping lithification front within the accretionary wedge or by both the presence and geometry of older, accreted, indurated sediments [*Byrne and Hibbard*, 1987]. Other suggestions for landward vergence have included low basal shear stress, a young subducting plate, high sedimentation rate, and a low/medium rate of convergence [*Seely*, 1977; *MacKay*, 1995; *Wang and Davis*, 1996; *Gulick et al*., 1998; *Gutscher et al*., 2001].

Coulomb wedge theory has been used to show that accretionary wedges at critical state have seafloor slope angles and dip angles of the basal shear plane that are a function of wedge interior strength and basal shear stress [*Davis et al*., 1983; *Wang and Hu*, 2006]. Offshore of northern Sumatra, the outer slope dip is 1.2°–1.8° [*McNeill and Henstock*, 2014] and the basal dip is 3°–5° [*Singh et al*., 2012], suggesting that this wedge is in a subcritical state [*Davis et al*., 1983]. A subcritical wedge will deform internally to form a steeper taper but not slide along its base until it achieves a critical state. Conversely, within 50 km from deformation front, the slope angle is 3.3°–3.9° [*McNeill and Henstock*, 2014], which suggests that the taper there is in a critical state [*Davis et al*., 1983]. For a wedge with continuing accretion at the toe, which is true for northern Sumatra, such a critical state means that the wedge is always deforming internally and sliding along its base to maintain its critical taper.

Other studies have proposed a strong wedge interior off northern Sumatra from observation of shallow thrust faults near the deformation front [*Mosher et al*., 2008] and extended landward vergent fold structures, suggestive of both thick and indurated incoming sediments [*Karig*, 1977; *Henstock et al*., 2006; *Dean et al*., 2010; *Gulick et al*., 2011]. Several seismic studies have attempted to map the wedge interior, proposing the existence of backstops of varying geometry. For example, *Chauhan et al.* [2009] and *Singh et al.* [2012] (Figure 1) have interpreted a back thrust which they argue formed the seaward edge of a backstop. This proposed back thrust extends seaward from the western edge of the Aceh Basin, following the ~5 km/s velocity contour at ~4 km depth, before deepening to cross a 6 km/s velocity region at ~18 km depth. Farther southeast, *Klingelhoefer et al.* [2010] (Figure 1) proposed a backstop under the Simeulue Basin based on seismic velocity of 6.3 km/s at ~6 km depth, which defines the proposed backstop roof, while a 6.8 km/s region at ~21 km depth defines its base. Around Simeulue Island, *Tang et al.* [2013] have also proposed a backstop defined by a roof velocity of 6 km/s at ~8 km depth under the Simeulue Basin, with a dip to ~17 km depth seaward of Simeulue Island.

Our study area is within the southern end of the 2004 rupture zone. Underlying structures differ between the 2004 and 2005 rupture zones [*Kopp et al*., 2008; *Dean et al*., 2010; *Shulgin et al*., 2013], so we do not attempt to extrapolate our results to the south. In our study area (Figure 1), a wide plateau has already been hypothesized to represent a strong prism formed by thick, ~4.5 km, sand-/silt-prone sediments that have dewatered/lithified near the accretionary front [*Dean et al*., 2010; *Gulick et al*., 2011; *Geersen et al*., 2013]. Another seismic study has also proposed that northern Sumatra accretionary prism contains strong inner wedge material, as expressed by seismic observations of both short- and long-wavelength folds between two prominent fore-arc highs, along with deformation that apparently occurs only within the youngest sediments near the Sunda Trench [*Fisher et al*., 2007]. Such a strong prism would allow for a seaward expansion in the updip limit of seismogenesis, with resultant increased tsunamigenic potential. Bathymetric observations by *Henstock et al.* [2006], and visual results from remotely operated vehicle dives [*Moran et al*., 2005] confirming the existence of folds and fault-generated scarps at the deformation front, further support the possibility of surface rupture(s) near the Sunda Trench axis.

3. Data

Information used for this research consists of multibeam bathymetric and MCS data acquired after the 2004 earthquake. Compiled bathymetric data from various cruises (Table 1) are synthesized in Figure 1. These data were acquired between 2005 and 2009 by The University of Texas at Austin (UT, USA), The British Royal Navy

Table 1. Cruises Acquiring Multibeam Data Compiled and Merged for This Investigation

Research Vessel	Cruise Designation	Dates of Acquisition	Multibeam	System Information
HMS Scott of the UK Royal Navy	Marine Scientific Research	Jan–Feb 2005	SASS IV	two sonar arrays operating at 12 kHz, outer beam at 50°–60°, 361 beams, and 120° swath width.
Marion Dufresne II	MD 149	Jul–Aug 2005	SeaFalcon 11	Echosounder operating at 12 kHz, 400–500 beams, and swath width of 120°.
Sonne	184/2	Aug 2005	SIMRAD EM 120	two transducers operating at 12 kHz, angular coverage <150°, and 191 beams/ping. Emission beam is 2° along track.
	186/1a-186/1c	Oct–Nov 2005		
	186/1d	Jan 2006		
	186/2-186/3	Jan–Mar 2006		
	189/1-189/2	Aug–Oct 2006		
	198/1-198/2	May–Aug 2008		
	200/1-200/2	Jan–Mar 2009		
Natsushima	NT05-02	Feb–Apr 2005	SeaBat 8160	A transducer array operating at 50 kHz, 126 beams, and a cross-track beam width 1.5° at nadir
Roger Revelle	Knox05RR	May–Jun 2007	SIMRAD 120	two transducers operating at 12 kHz, angular coverage <150°, and 191 beams/ping. Emission beam is 2° along track.

(United Kingdom), Oregon State University (USA), Institut Français de Recherche pour l'Exploitation de la Mer (France), Bundesanstalt für Geowissenschaften und Rohstoffe (BGR) (Germany), and Kyoto University (Japan). The merged bathymetric data have a 50 m grid resolution spacing and extend over the entire fore arc, from northwest of northern Sumatra to west of Simeulue Island.

MCS data used in this study are a combination of data acquired by BGR during *Sonne*-186/2 (25 January to 15 March 2006) and by UT during *Sonne*-198/2 (18 July to 1 August 2008; designated SUMUT). The red lines in Figure 1 represent seven MCS profiles interpreted for this investigation. Different MCS systems were utilized. The SUMUT survey acquired 1250 km of data using a source array of 12 G-guns (total volume 5420 in^3), a 2.4 km long streamer containing 192 channels, and streamer depth of 10 m. Shot interval was 20 s ± 0.2 s. SUMUT recorded 16 s of MCS data with a 2 ms sampling interval. The BGR survey used a source array consisted of 16 G-guns divided into two subarrays; total volume was 3100 in^3. The 3 km long streamer consisted of 240 channels with a receiver spacing of 12.5 m, towed at a depth of 6 m. The shot interval was 18 s ± 0.3 s, and 14 s of MCS data were recorded with a sampling interval of 2 ms.

4. Methodology

For the bathymetry, we used CARIS HIPS and SIPS to clean and merge all available bathymetric data (Table 1). Prior to editing, these data were set to a horizontal resolution of 50 m, a depth resolution of 1 m, a scale of 1:10,000, and the projection datum was universal transverse Mercator (UTM)-World Geodetic System 84, zone UTM 46N. We cleaned the data interactively, visually inspecting for outliers and artifacts, line-by-line and swath-by-swath. A depth file produced by CARIS was read by the Generic Mapping Tools [*Smith and Wessel*, 1990; *Wessel and Smith*, 1991, 1998] to generate the merged bathymetric map (Figure 1).

We processed the MCS data through poststack time migration, with targeted areas reprocessed through prestack time migration. Further processing detail is presented in *Gulick et al.* [2011] and *Martin et al.* [2014]. The BGR MCS data have been presented by *Berglar et al.* [2010], where each seismic profile is processed through poststack Kirchhoff time migration. Figures 2–4 show seismic profiles used in this study. All of these profiles are shown in two-way travel time (ms), as shown along the vertical axes.

5. Observations

5.1. Bathymetry

The accretionary prism offshore of northern Sumatra is composed of a wedge up to ~180 km wide [*Fisher et al.*, 2007], water depth from ~4.5 km [*Gulick et al.*, 2011] near the Sunda Trench to <1 km on the fore-arc high west of the Aceh (fore-arc) Basin. The Aceh Basin has a maximum depth of ~2.5 km [*Berglar et al.*, 2010]. In the south, the wedge narrows to ~125 km around Simeulue Island. Landward of the deformation

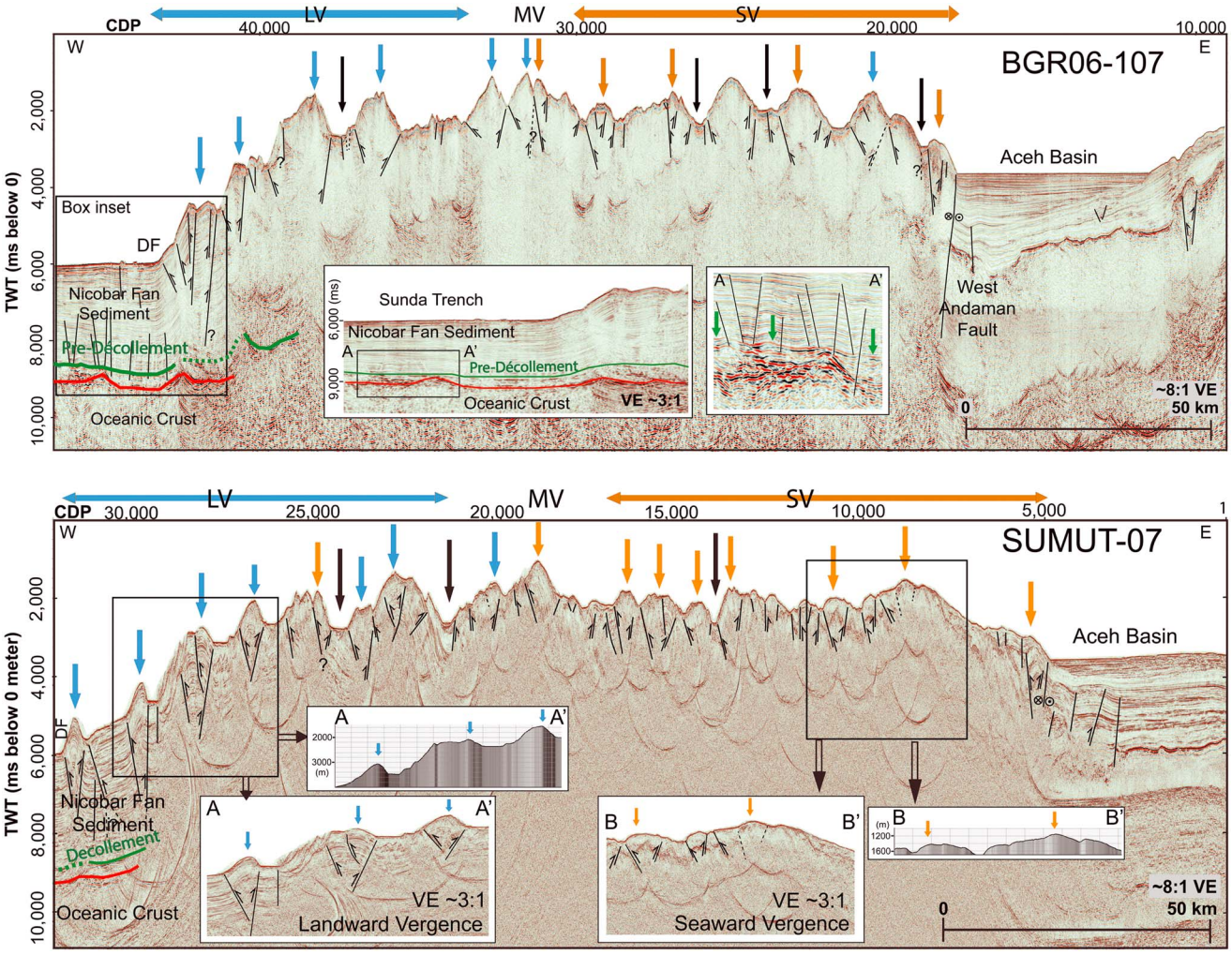

Figure 2. Interpreted seismic profiles (a) BGR06-107 and (b) SUMUT-07. See Figure 1 for locations. Figures 2 and 3 are interpreted seismic profiles with vertical exaggeration ~8 and ~3 for Figure 4. Uninterpreted profiles with lower vertical exaggeration are submitted as supporting information with some subsets showing interpreted faults. On all profiles, CDP number (upper margin) shows the distance along the length; travel time depth is shown on the left (ms). The green line is interpreted predécollement, the red line is interpreted top of oceanic crust, and DF stands for deformation front. The vertical blue, orange, and black arrows indicate interpreted landward vergent folds, seaward vergent folds, and piggyback basins, respectively. Our interpreted vergence zone widths are shown with colored horizontal arrows. The horizontal blue arrows (Figure 2a: CDPs ~33,000–43,000 and Figure 2b: CDPs ~21,000–32,000) represent interpreted landward vergence. The horizontal orange arrows (Figure 2a: CDPs ~18,000–30,000 and Figure 2b: CDPs ~5,000–17,000) represent interpreted seaward vergence. Between these two vergence zones (Figure 2a: CDPs ~30,000–33.000 and Figure 2b: CDPs ~17,000–21,000) is a region of mixed vergence. Inset figures in Figure 2a show interpreted blind normal faults that crosscut the interpreted predécollement. Two inset pairs in Figure 2b show bathymetric and seismic data of interpreted landward and seaward vergent folds in lower VE.

front, over an along-strike width of ~20–30 km offshore of Simeulue Island, is a region with steep slopes interpreted as the result of widespread surface erosion; these slopes are steeper than those defined by fold flanks farther landward [*Kopp et al*., 2008].

Merged bathymetric data reveal that the accretionary wedge is composed of lineated highs and lows oriented primarily along margin strike [*Graindorge et al*., 2008], with distances of 2–15 km between topographic highs. The widths of the highs are 2–45 km; intervening troughs are 1–8 km wide. Relief of these topographically high regions can be as much as ~1500 m. Dominant along-strike trends of the highs are ~320° in the north and ~290° in the south (Figure 1). For comparison, the deformation front strikes ~330° in the north and ~310° in the south.

We use the compiled bathymetric data to estimate presumed fold vergence by first comparing the steepness of slope flanks within each lineated high, then by checking subsurface structure beneath these highs using the MCS data. Using both the seismic and seafloor data reduces uncertainties regarding the 3-D relationships

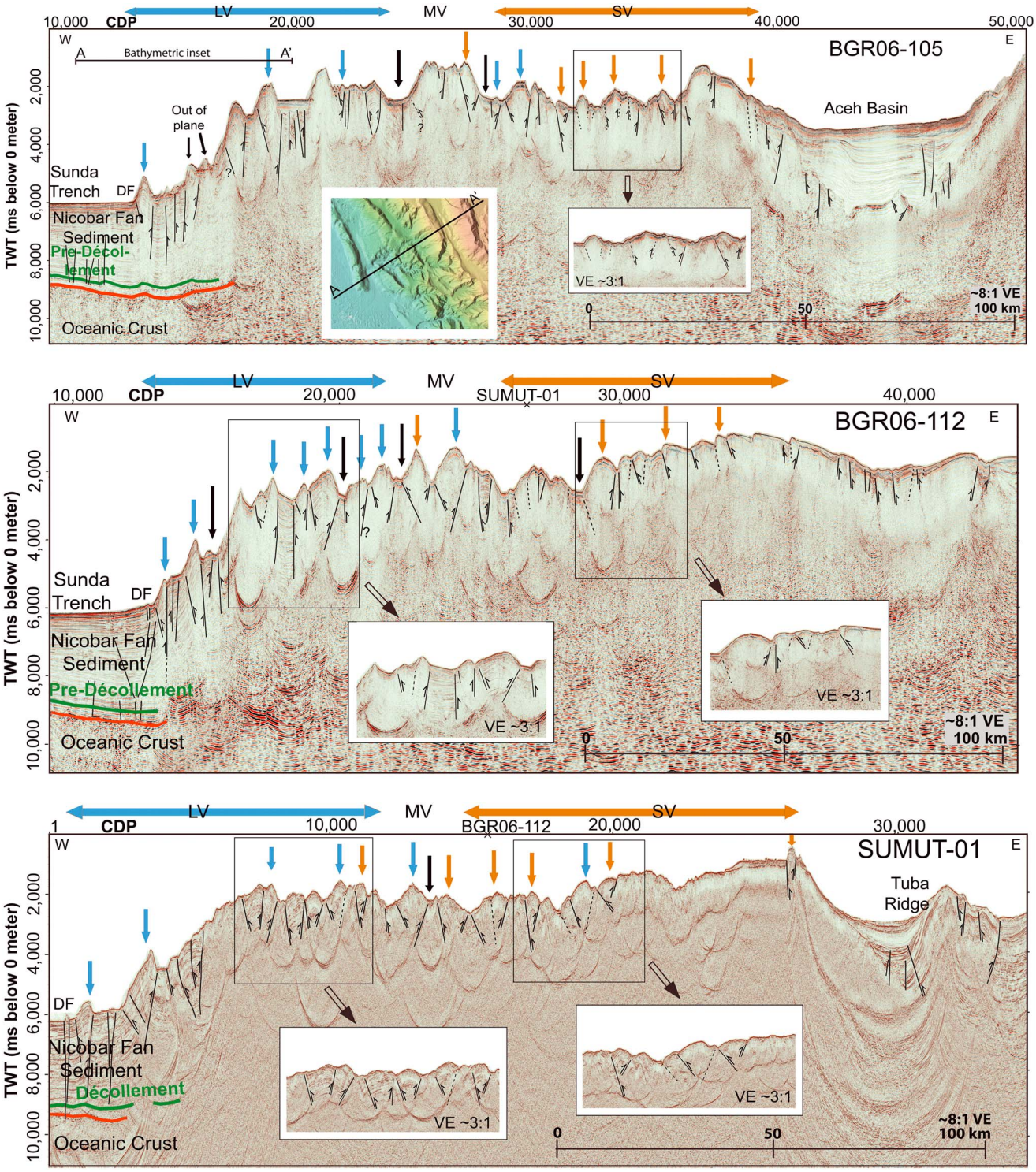

Figure 3. Interpreted seismic profiles (a) BGR06-105, (b) BGR06-112, and (c) SUMUT-01. See Figure 1 for locations and caption of Figure 2 for description of annotations. The horizontal blue arrows (Figure 3a: CDPs ~13,000–25,000; Figure 3b: CDPs ~13,000–22,000; and Figure 3c: CDPs ~1,000–11,000) represent interpreted landward vergence regions. The horizontal orange arrows (Figure 3a: CDPs ~29,000–40,000; Figure 3b: CDPs ~26,000–36,000; and Figure 3c: CDPs ~15,000–26,000) represent interpreted seaward vergence zones. The region between the two (Figure 3a: CDPs ~25,000–29,000; Figure 3b: CDPs ~22,000–26,000; and Figure 3c: CDPs ~11,000–15,000) is characterized by mixed vergence. Inset figure in Figure 3a shows bathymetric data around the prism toe of massive slope failures. Subsets of seismic data shows interpreted thrust faults with certainty and less certainty (dashed).

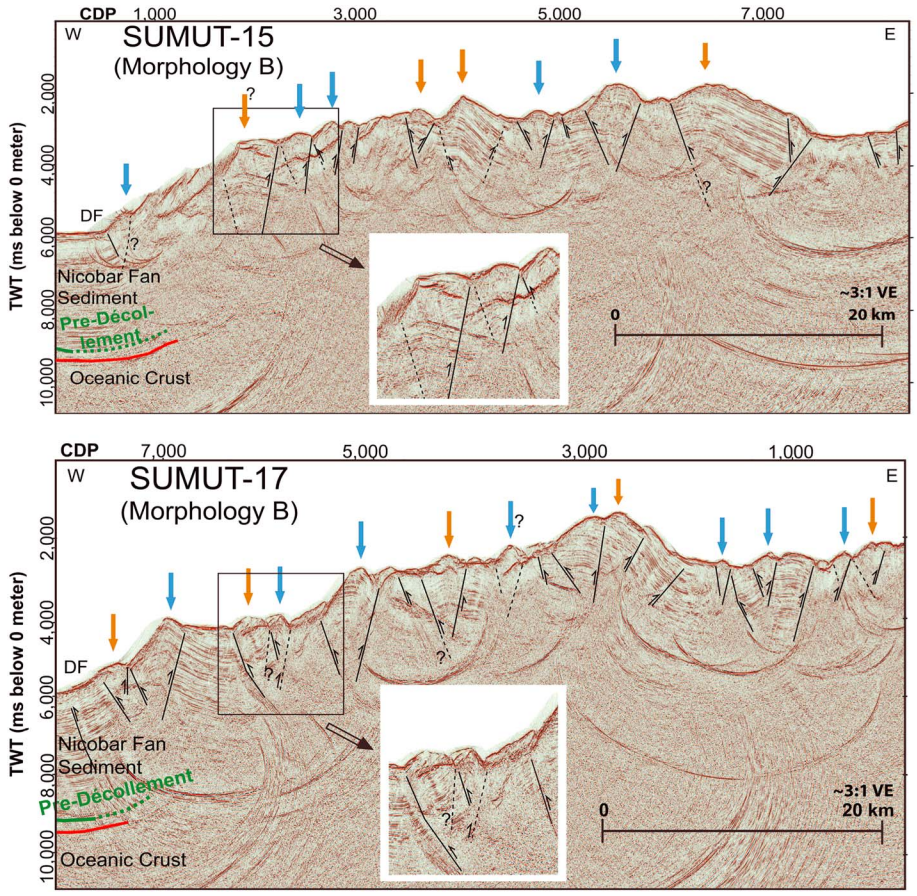

Figure 4. Interpreted seismic profiles (a) SUMUT-15 and (b) SUMUT-17. See Figure 1 for locations and caption of Figure 2 for description of annotations. These profiles transect morphology B [*Henstock et al.*, 2006], where the prism toe consists of a frontal fold with erosion. The lengths of these profiles are ~50 km. Both exhibit predominantly landward vergence (Figures 1 and 5). Subsets of seismic data show interpreted thrust faults and an example of faults interaction that probably cause the seaward vergent fold.

of subsurface folds and seafloor slopes. In all cases, we assume that the steeper seafloor slope associated with a fold indicates that fold's vergence direction (Figure 2b inset). We acknowledge that steeper slopes may also be the result of surficial erosion, a result of higher-order (i.e., minor) thrust faults and/or interactions between folds. To reduce this uncertainty, we verified the existence of thrust fault(s) underlying the steeper slope at the base of observed folds. Using the available MCS data (Figures 2–4), we can therefore both validate fold vergence and interpret shallow faults flanking such folds, if they exist at the resolution of our seismic data (Figure 2b insets; see next section). Furthermore, we use dashed lines and/or question marks to represent faults interpreted with less certainty (Figures 2–4; Figures 3a and 4b insets). We used blue and orange vertical arrows for landward and seaward vergent folds, respectively. Some folds are without any arrow, because of uncertainty. *Graindorge et al.* [2008] measured slope gradients on their bathymetric data within the region 1.5–6°N and 92–96°E in order to determine fold vergence; our zone of predominant landward vergence zone is comparable to theirs.

5.2. MCS Data

Available MCS profiles (Figure 1, seven red lines) image the upper 1–2 s of the wedge, illustrating that it is affected by complex landward and seaward dipping interpreted fault planes. These fault planes generally bound the higher and lower regions observed on the bathymetric data. We interpret the highs as lineated anticlinal structures, exhibiting separations of 2–15 km, between what we interpret as first-order (major) thrust faults and paired conjugate structures; second-order (i.e., smaller-scale) faults are generally separated by $<$1 km, occurring generally within these anticlines. We base our interpretation of any fold's direction of

shortening on the related interpretation of vergence and primary versus back thrust relationships of interpreted thrust faults flanking each fold (Figure 2b inset). Near the Sunda Trench, we can interpret normal faults down to ~8.8 s two-way travel time, the depth of our interpreted predécollement (Figures 2–4, green line; Figure 2a inset). We interpret the predécollement based on its negative polarity (Figure 2a inset, green arrows). Near the trench, the interpreted landward vergent fold is an example of fault interaction resulting in the observed landward verging thrust fault that possibly extends toward the décollement (Figures 2 and 3). Within the plateau landward of the trench, faults are harder to identify >2 s below seafloor. We acknowledge that Figures 2–4 are shown with high vertical exaggeration (VE) in order to show greater lateral extents; therefore, we provide subsets with lower VE. Uninterpreted profiles using lower VE are submitted as supporting information with subset figures showing interpreted faults.

5.2.1. Seismic Profiles BGR06-107 and SUMUT-07

SUMUT-07 (Figure 2b) is approximately parallel to and ~34 km south of BGR06-107 (Figures 1 and 2a). Along these profiles, seafloor depths range from ~4500 m near the trench to ~990 m (common depth point (CDP) ~31,800; Figure 2a) and ~750 m (CDP ~19,000; Figure 2b), ~75 km and ~90 km, respectively, landward from the trench. The widths of the accretionary prism along these profiles are ~165 km (Figure 2a) and ~185 km (Figure 2b), respectively. We interpret the predécollement at subsurface depths ranging from ~8.8 s (CDP 46,500; Figure 2a) beneath the Sunda Trench to ~8 s (CDP ~39,300; Figure 2a) to ~9 s (CDP 32,000; Figure 2b) beneath the deformation front [*Dean et al*., 2010]. From the deformation front to the seaward edge of Aceh Basin, spacing of interpreted anticlines and intervening synclines ranges from ~2 to 13 km. Widths of these folds at the seafloor range from <1 to 12 km. Near the trench (Figure 2a inset), several blind (i.e., nonsurfacing) normal faults appear to intersect the predécollement. The first fold landward of the trench is landward vergent (CDP ~42,500); it is an example of fault interactions where the observed major thrust fault possibly extends toward the décollement. Five more interpreted landward vergent folds are observed from the trench into the prism. The width of this landward vergent zone is ~65 km. The westernmost seaward vergent fold occurs at CDP ~31,800, which is also the shallowest part of the wedge on BGR06-107. Toward the Aceh Basin to the east, interpreted folds are predominantly seaward vergent. The width of the seaward vergent zone is ~80 km. A region of mixed vergence, ~25 km wide, occurs in between, from CDP ~30,000 to ~33,000. We acknowledge that the widths of these vergence zones are an approximate; they represent the span of prevalent vergence direction of folds as confirmed by images of subsurface faulting. For the mixed vergence zone, we estimated its width to encompass the area with fold(s) of both vergence styles (no preferred vergence) bounded by local troughs. In Figure 2b, near the westernmost landward vergent fold (CDP ~31,500), we interpret blind faults extending downward toward the predécollement. A generally landward vergent zone again occurs nearer the deformation front (CDP ~21,000–32,000), with a width of ~75 km, and a seaward vergent region extends from CDP ~17,000 for ~90 km toward the Aceh Basin. The fold near CDP ~19,000, interpreted as seaward vergent, occurs at the shallowest part of the wedge, within a mixed vergence zone ~25 km wide. Piggyback basins (Figure 2a: CDPs 37,700; 26,000; 24,500; and 19,000 and Figure 2b: CDPs 24,500; 21,500; and 14,000) are observed scattered across the plateau; in all cases, fanning of infilling sediment suggests syntectonic deposition and continuing compression of fill within these basins [*Sibuet et al*., 2007]. We interpret the West Andaman Fault along the western/seaward edge of the Aceh Basin (Figure 2a) [*Sibuet et al*., 2007; *Martin et al*., 2014]. Within the Aceh Basin itself, blind faults appear to crosscut an acoustically strong reflector at ~6 s. *Berglar et al.* [2010] and *Martin et al.* [2014] interpret this strong reflector as the acoustic basement of the Aceh Basin.

5.2.2. Seismic Profiles BGR06-105, BGR06-112, and SUMUT-01

Interpreted MCS profile BGR06-105 (Figure 3a) is located ~10 km south of SUMUT-07 and approximately parallel to it (Figures 1 and 2b). Seismic profile BGR06-112 (Figure 3b) is located ~85 km south of and is approximately parallel to BGR06-105 (Figures 1 and 3a). Seismic profile SUMUT-01 (Figure 3c) crosses the accretionary prism at an ~70° angle (Figure 1). In its southwestern portion, this profile is ~120 km south of BGR06-105, but its northeastern end is only ~34 km south of BGR06-105. Profile SUMUT-01 crosses BGR06-112 at CDP 26,500 (Figure 3b). Profile BGR06-112 crosses SUMUT-01 at CDP 15,600 (Figure 3c). Figure 3 exhibits seafloor depths ranging from ~4500 m near the trench (Figure 3a: CDP 10,000; Figure 3b: CDP 10,000; and Figure 3c: CDP 1) to ~600 m (Figure 3a: CDP 25,400 and Figure 3b: 34,750) within the prism and locally only ~270 m (Figure 3c: CDP 26,300) near the Tuba Ridge [*Malod et al*., 1993; *Curray*, 2005; *Mosher et al*., 2008; *Martin et al*., 2014]. In Figure 3 (profiles BGR06-105, BGR06-112, and SUMUT-01), we interpret the predécollement to be at depths ranging from 8.2 to 9 s [*Dean et al*., 2010]; near the trench, we interpret

"blind" normal faults extending down to the predécollement. The spatial distribution of observed vergence regions is similar to that shown by BGR06-107 (Figure 2a) and SUMUT-07 (Figure 2b); predominantly landward and seaward vergence zones exist (Figure 3). We observe at least one piggyback basin on each of these profiles (Figure 3a: CDPs 25,000 and 28,000; Figure 3b: CDP 15,600, 20,100, 22,100, and 28,400; and Figure 3c: CDP 13,500). In all observed piggyback basins, we presume continued shortening [*Sibuet et al*., 2007] of the prism, as they are filled by tilted sedimentary strata.

On profile BGR06-105 (Figure 3a), landward from the trench, between the first and second landward vergent folds (CDP 13,500 and 18,700, respectively), two isolated folds appear to be seaward vergent (CDP 15,600 and 17,500). The seaward facing sides of these folds appear to be eroded [*Mosher et al*., 2008], as shown by rough surface texture on the bathymetry data (Figure 1 and Figure 3a inset). Because their appearance has been modified by surficial erosion, we suggest that both of these folds are landward vergent. Upon examination of the bathymetric data, the symmetrical fold adjacent to the interpreted fold at CDP 15,600 looks instead to be an artifact of the data acquisition (an out-of-plane image), and we conclude therefore that it cannot be used to discern vergence. Zoomed-in figure in Figure 3a shows our fault interpretation; the dashed lines represent less certainty, and the solid lines represent greater certainty.

Profiles BGR06-112 (Figure 3b) and SUMUT-01 (Figure 3c) cross the plateau landward from a region of folded structures near the trench to a topographically higher region with less apparent near-surface deformation (starting at CDP ~30,000 (Figure 3b) and at CDP ~19,000 (Figure 3c)). This elevated, smooth region (Figure 1, dashed brown trapezium) lies northwest of and on-strike with Simeulue Island. Other islands farther southeast along this margin are known to be capped by Quaternary carbonate reefs [*Dorobek*, 2008]. Furthermore, the Simeulue Basin, eastward of Simeulue Island, is known to contain multiple carbonate platforms [*Berglar et al*., 2008; *Lutz et al*., 2011]. Based on the proximity of such platforms, its relatively flat top, the pinnacle-like feature on SUMUT-01, and the lack of acoustic penetration associated with it, we conclude that this region is a shallowly submerged carbonate platform. Subsets in Figures 3b and 3c show some preserved block-like strata forming the folds where we can interpret faults with confidence.

5.2.3. Seismic Profiles SUMUT-15 and SUMUT-17

Figure 4 shows two ~50 km long seismic profiles, SUMUT-15 and SUMUT-17 (Figure 1). Based on negative polarity, we interpret a predécollement surface on SUMUT-15 at ~9 s (CDP 0) to ~8.5 s (CDP 1200) and on SUMUT-17 at ~9 s (CDP 8000) to ~8 s (CDP 7000). All interpreted faults are within ~2 s of seafloor. *Henstock et al.* [2006] have proposed two different morphology zones along this part of the deformation front, which they designate A and B, based on topographic distinctions near the toe of slope. They interpret morphology A to be the result of a seaward dipping thrust fault, yielding a landward vergent fold; conversely, morphology B implies the presence of a landward dipping thrust fault, causing a seaward vergent fold. The five profiles shown in Figures 2 and 3 transect a seafloor region along the deformation front which has been interpreted as morphology A [*Henstock et al*., 2006]. Conversely, the profiles in Figure 4 intersect the deformation front called morphology B [*Henstock et al*., 2006]. Subsurface fault interpretations of SUMUT-15 (Figure 4a) show that the region landward of morphology B can be interpreted as predominantly landward vergent. However, observations along SUMUT-17 (Figure 4b) show an increased number of seaward vergent folds on that profile. Subset in Figure 4a shows a fold interpretation uncertainty due to apparent surface erosion. Inset in Figure 4b displays faults interaction and uncertainty in interpretation; both fold vergence styles are observed.

6. Discussion

6.1. Seafloor Morphology

Observed lineations of bathymetric highs show changes of direction between northern and southern parts of the fore arc (Figure 1). In the northern portion, the prism toe exhibits generally smooth fold and trough topography [*Henstock et al*., 2006]. Conversely, the southern part of the toe region is characterized by more slope failures, resulting in more rugged, shorter-wavelength topography [*Kopp et al*., 2008]. Structural trend of the deformation front is 330° in the northern portion and 310° in the south. However, the strike of fault-controlled ridges landward of the deformation front is ~320° in the northern section and is ~290° in the southern. We suggest that these differences in strike between the deformation front and ridges within the plateau, amounting to ~10° in the northern region and ~20° in the southern part, are the result of slope failures

occurring along the deformation front, which occur more extensively in the southern portion of the study area (Figure 1). Frontal slope failures may occur when initial underthrusting of sediments at the deformation front produces oversteepening of the slopes [*Kopp et al*., 2008]. The along-strike change of structural trend has also been observed by *Dean et al.* [2010] and *McNeill and Henstock* [2014], near where the 96°N fracture zone is subducting (~2.5°N). They have pointed out a difference both in prism width and in taper angle north and south of this intersection and conclude that smoothness of the subducting plate, along with sediment thickness and properties, play roles in the differing prism morphology observed.

6.2. Wedge Morphology and Structure

Seismic profiles BGR06-107, SUMUT-07, BGR06-105, BGR06-112, and SUMUT-01 (Figures 2 and 3) image the accretionary prism over along-strike distances of ~180 km near the deformation front and ~140 km near the seaward edge of the Aceh Basin. Observed changes in seafloor topography illustrate the complex shallow structure of the prism. Folding and associated bounding thrust faults dominate the upper 1–2 s subseafloor of prism structure. Fold spacing on all profiles is similar, ~2–15 km between axes, with fault spacing 1–7 km. Between some anticlines lie piggyback basins; tilted strata within these basins, extending to the modern seafloor, suggest that bounding thrust faults have been recently active and that compression continues across the study area, although timing of onset of deformation is uncertain [*Sibuet et al*., 2007; *Graindorge et al*., 2008]. Such piggyback basins are inferred by others as close as ~10 km from the deformation front [*Kopp et al*., 2008] south of our study area and as far as ~100 km from the deformation front [*Fisher et al*., 2007] to the north.

Both extant theories and experiments suggest that the observed extensive landward vergence may occur by any one or a combination of five boundary conditions: (1) low basal shear stress, (2) a seaward dipping lithification front/backstop, (3) high sedimentation rate, (4) young subducting plate, and/or (5) low/medium rate of convergence [*Seely*, 1977; *Byrne and Hibbard*, 1987; *MacKay*, 1995; *Wang and Davis*, 1996; *Gulick et al*., 1998; *Gutscher et al*., 2001]. Using seismic observations along the Sunda subduction zone, *McNeill and Henstock* [2014] propose that landward vergence zone near the prism toe offshore of northern Sumatra may be due either to low basal shear stress or the presence of a backstop; they observe acoustic evidence of an overpressured layer at depth that has become predécollement (Figure 2a inset) [*Dean et al*., 2010; *Geersen et al*., 2013]. There is no consensus on age of the subducting plate; proposed ages range from 52–61 Myr [*Singh et al*., 2011] to 21–24 Myr [*Müller et al*., 2008]. The rate of convergence is 5–6 cm/yr [*Natawidjaja et al*., 2007], a low-medium range. Therefore, the relevant boundary conditions for landward vergence offshore of northern Sumatra include boundary conditions 1–3. The prevalence of extended landward vergence east of the deformation front (Figure 5) also suggests that high sedimentation rate is an important controlling variable, as we observe ~4.5 km thick incoming sediment everywhere along this portion of the Sunda Trench (Figures 2–4). Seaward vergence dominates farther south, where incoming sediments are thinner [*Kopp and Kukowski*, 2003; *Gulick et al*., 2011; *McNeill and Henstock*, 2014; *Moeremans et al*., 2014].

One consequence of thick incoming sediment, particularly fan-based sediment that may be sand-/silt-prone, is that coarser-grained material could accelerate dewatering and associated lithification at depth [*Gulick et al*., 2011; *Geersen et al*., 2013]. Near the deformation front, we observe blind normal faults that crosscut the predécollement at depths of 8–9 s (Figures 2 and 3); we suggest that these faults form fluid conduits as deeper layers undergo lithification prior to accretion [*Gulick et al*., 2011]. Sediments >2–3 km thick that extend over large distances can also trigger dewatering processes before accretion, through increased temperature-driven diagenetic activity [*Geersen et al*., 2013]. In our seismic profiles, we also suspect induration of shallower wedge sediments because of observed preservation of block-like layering landward of the deformation front (Figures 2b, 3b, and 3c insets) [*Gulick et al*., 2011], along with a general lack of acoustic penetration deeper than ~2 s farther landward (Figures 2–4). We suggest that these incoming (sediment) blocks have been dewatered and lithified before being accreted, contributing to the strength of the associated wedge interior [*Gulick et al*., 2011; *Geersen et al*., 2013].

Northwest of our study area (Figure 1), *Fisher et al.* [2007] have studied a portion of the wedge plateau >100 km wide that is topographically depressed in the center; such a pattern is not representative of the general morphology of the plateau within our study area. On three of our crossing profiles (Figures 2a, 2b, and 3a), we instead observe the shallowest point to be within the plateau, while on two other profiles (Figures 3b and 3c), we observe a topographic high, ~60 km wide, with apparently reduced deformation,

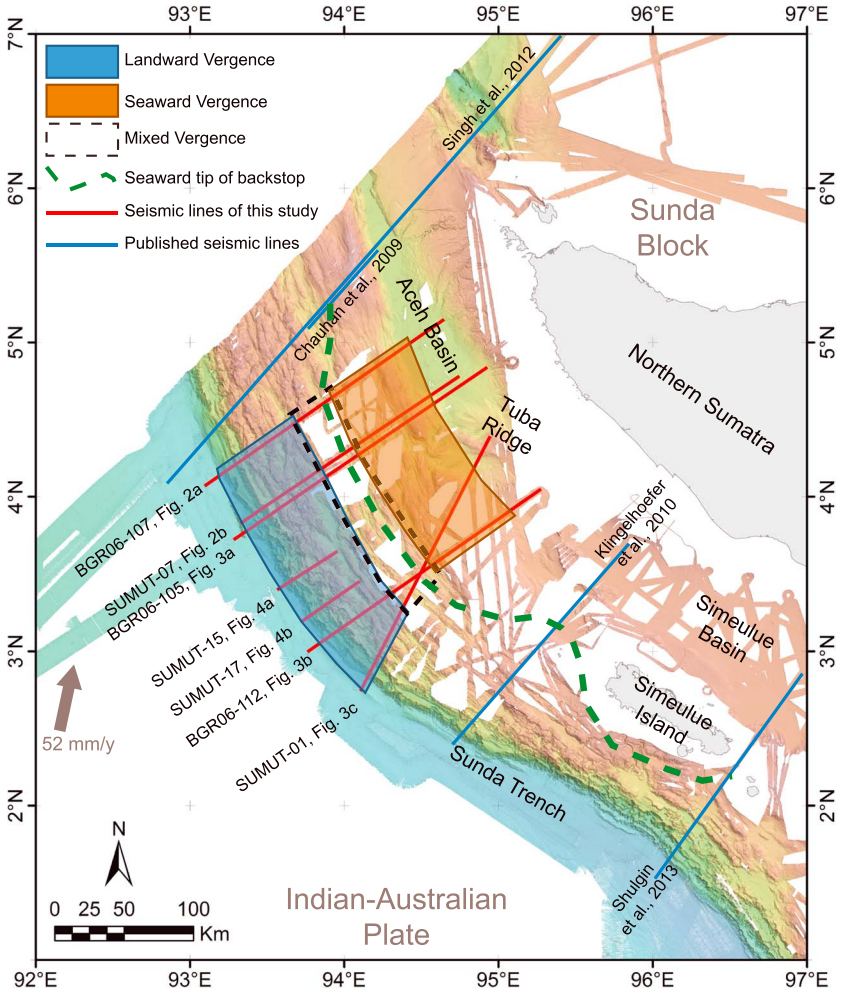

Figure 5. Structural classification based upon analysis of the seven seismic profiles (red lines) imaging the northern Sumatra accretionary prism (Figures 2–4). The blue polygon represents landward vergence zone, and the orange polygon represents seaward vergence zone. The mixed vergence zone (dashed polygon) lies in between. The dashed green line is our proposed seaward tip (edge) of the rigid backstop that we propose for this part of the wedge.

adjacent to the Aceh Basin. *Fisher et al.* [2007] have suggested that the wide, approximately flat plateau implies a strong wedge interior. The observed steep wedge taper at the deformation front (8°–12° seaward slope of the outer high, 5° dip of the basal décollement [*Fisher et al*., 2007]) narrows landward of the outer high, which is also consistent with increased strength of the wedge interior [*Davis et al*., 1983; *Wang and Hu*, 2006]. In comparison, our seismic profiles consistently show both an extended region of landward vergent folds (Figure 5) and a plateau-wide limit of penetration of ~2 s that may reflect accreted sediment at depth deformed sufficiently to disrupt sedimentary layering. We suggest that these observations also support a strong wedge interior.

In our observations (Figures 2 and 3), the region landward of the trench (bathymetry morphology A) is predominantly landward vergent, supporting the hypothesis for that morphology, a seaward dipping frontal thrust, put forward by *Henstock et al.* [2006]. However, Figures 4a and 4b also support predominantly landward vergence within ~50 km of the deformation front landward of morphology B, contradicting *Henstock et al.* [2006] that such a morphology should be caused by a landward dipping thrust fault. Our observations, and existing published studies, all confirm that the thickness of incoming sediment is the same throughout our study area. Our seismic observations support an approximately constant predécollement depth beneath the deformation front. Therefore, we conclude that the wedge's interior structure must be consistent along strike from 2.5–4.5°N, supporting the existence of seaward dipping thrust faults (i.e., landward vergence) everywhere along the deformation front within this region (Figure 5) [*McNeill and Henstock*, 2014].

Table 2. Widths of Vergence Zones Along Strike (Refer to Figure 1b)

	Landward Vergence (km)	Seaward Vergence (km)	Mixed Vergence (km)
BGR06-107 (Figure 2a)	~65	~80	~25
SUMUT-07 (Figure 2b)	~75	~90	~25
BGR06-105 (Figure 3a)	~63	~75	~24
BGR06-112 (Figure 3b)	~55	~90 (include the topography high)	~22
SUMUT-01 (Figure 3c)	~69	~80 (include the topography high)	~23

Our five cross-wedge profiles (Figures 2 and 3) exhibit approximately the same tripartite division of vergence zones: landward vergent on seaward side nearer the deformation front, mixed vergence in the middle, and seaward vergence nearer the Aceh Basin [*McNeill and Henstock*, 2014]. However, the observed widths vary along strike (Table 2). Figure 5 displays a map view summary of the three zones. The zone of mixed vergence includes the shallowest point on the wedge for three of the five cross wedge seismic profiles: BGR06-107 (~1000 m, CDP ~31,800; Figure 2a), SUMUT-07 (~1000 m, CDP ~19,000; Figure 2b), and BGR05-105 (~1100 m, CDP ~27,000; Figure 3a). On the other two cross-wedge profiles, the shallowest point of the wedge corresponds to the topographically elevated, smooth region (Figures 3b and 3c) within the seaward vergence zone that we have already surmised represent drowned carbonate platforms capping the wedge topography/structures [*Dorobek*, 2008] possibly with some addition vertical tectonics from the adjacent West Andaman Fault [*Martin et al*., 2014].

6.3. Proposed Backstop Model

A backstop, a distinctive structure within an accretionary prism that is stronger than the subsequent/younger accreting material, represents a buttress against which accreting material deforms [*Davis et al*., 1983; *Byrne et al*., 1993]. Our study of the accretionary prism offshore of northern Sumatra shows that a landward vergence zone is consistently situated landward of the deformation front for a cross-wedge distance up to ~75 km (Table 2). Based upon what is proposed from numerical models and sandbox experiments as to how such landward vergence develops [*Davis et al*., 1983; *Byrne et al*., 1993; *Gutscher et al*., 1998], we suggest the existence of a seaward dipping backstop within the wedge, east of the mixed vergence zone (Figure 5). We acknowledge that the location for the mixed vergence zone is potentially quite broad and our proposed backstop position is only approximate. The vergence interpretation of some faults is less certain in the center and rear of the wedge where structure and morphology is complex, seismic imaging is less clear, and the broadly coincident bathymetric high in the center of the plateau is, for some transects, topographically subtle.

Our proposed backstop geometry (Figure 6) lies between 2°N and 5°N, based on our interpretation of the structure and morphology of this part of the accretionary prism, backstop models in subduction settings [*Byrne et al*., 1993; *Gutscher et al*., 2001; *Storti et al*., 2001], and velocity models [*Klingelhoefer et al*., 2010; *Singh et al*., 2012; *Tang et al*., 2013]. For the northern region of our study area (Figures 1 and 6a), we use a velocity model published by *Singh et al.* [2012] as a basis for our backstop interpretation. We interpret the top of the backstop under the Aceh Basin to coincide with a velocity contour of ~5.8 km/s; this velocity represents a reasonable average velocity for continental (i.e., Sunda Block) crust [*Taira et al*., 1998; *Brocher*, 2005]. For the southern region (Figure 6c), we estimate the roof of our proposed backstop to approximate the ~5.8 km/s contour [*Klingelhoefer et al*., 2010]. As is true of all velocity models, uncertainty increases with depth. The 5.8 km/s contour may represent an average velocity of continental crust, but that and higher velocities could also represent older accreted material overlying continental crust.

For the central part of the prism in our study area (Figures 1 and 6b), we use SUMUT-07 (Figure 2b) as basis for our backstop interpretation; it represents the seven profiles we studied. SUMUT-07 crosses the Aceh Basin, where we observe a strong acoustic basement reflector at the base of the basin's presumed sedimentary fill. We hypothesize that the roof/top of the material that forms our proposed backstop coincides with that reflector, which occurs at a depth of ~6 s beneath the basin. We estimate this depth to coincide with the ~5.8 km/s contour generated by *Chauhan et al.* [2009], *Klingelhoefer et al.* [2010], *Singh et al.* [2012], and *Shulgin et al.* [2013] (Figure 1); the ~5.5 km/s contour generated by *Tan et al.* [2012]; and the strong basement reflector recognized by *Berglar et al.* [2010] in the same area. We cannot estimate either the roof position or slope of the backstop from the west end of Aceh Basin seaward beneath the wedge, since there is no recognizable

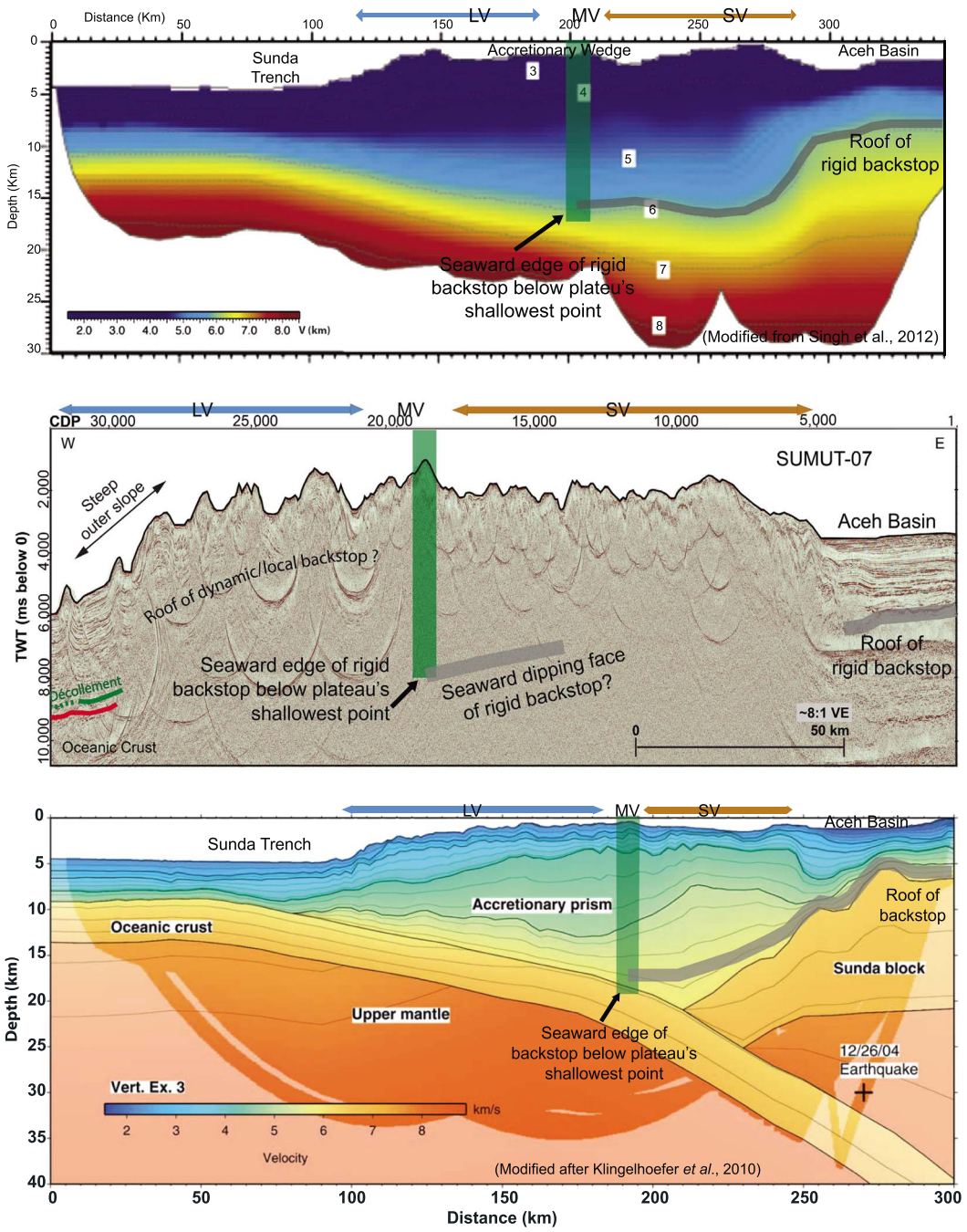

Figure 6. Proposed geometry of a backstop within the wedge for region 2–5°N. Refer to Figure 1 for location. The thick grey curves in all panels are estimated location and shape of the roof of our proposed backstop. The blue and orange horizontal arrows represent structural zones: landward vergence and seaward vergence. The mixed vergence zone is between the two zones. (a) Northern part based on a velocity model published by *Singh et al.* [2012]. Our proposed roof of the backstop follows the ~5.8 km/s (grey curve). The seaward tip of that backstop is located under the shallowest point of the wedge (green bar), which generally lies within our mixed version zone (Figure 5). (b) The central part of our study area. The roof of the proposed backstop coincides with a strong reflector under the Aceh Basin (grey curve) [*Berglar et al.*, 2010]. The seaward tip of the backstop is located under the shallowest point of the wedge (green bar). (c) The roof geometry of the backstop in the southern part based on a velocity model of *Klingelhoefer et al.* [2010]. Again, the roof of the backstop follows the ~5.8 km/s (grey curve). In general, we conclude that the roof of the backstop from the western edge of the Aceh Basin form a seaward dipping slope and extend into the wedge to the position under the shallowest point of the wedge (green bar).

reflector in this area. However, we can infer a likely geometry based on what is known from accretionary wedge modeling (Figures 6a and 6c), specifically results from sandbox experiments [*Byrne et al*., 1993; *Wang and Davis*, 1996; *Gutscher et al*., 2001] along with seismic observations from other parts of this margin [*Kopp and Kukowski*, 2003]. All indicate that for seaward dipping backstops, the shallowest point along a wedge likely coincides with the backstop's seaward toe or edge. The backstop geometry used in sandbox experiments or numerical models to simulate accretionary wedge evolution is generally either rectangular or triangular. In the rectangular case, both seaward and landward edges are vertical; the seaward edge acts like a snowplow, deforming younger incoming sediments [*Davis et al*., 1983], while the roof is horizontal [*Wang and Davis*, 1996]. In the triangular case, the bottom side rests along the landward dipping subducting plate and the seaward side forms a seaward dipping slope [*Byrne et al*., 1993]. The tip of the triangle between these two sides is located somewhere beneath the wedge, essentially a doorstop lying near or on top of the subducting plate. Model results show that the location of this tip can coincide with the location of the shallowest point of the accretionary wedge [*Byrne et al*., 1993; *Gutscher et al*., 2001]. Our proposed backstop incorporates these model results; we propose a generally seaward dipping backstop with a tip beneath the shallowest part of the prism (Figure 5, dashed green line).

We can identify the shallowest point on the wedge plateau on three of our five cross-prism profiles (Figures 2a, 2b, and 3a). In Figures 3b and 3c, interpreted shallow carbonate platforms within the seaward vergence zone lie above this backstop, obscuring what could be the tip of a backstop within our mapped mixed vergence zone. Nonetheless, we suggest that everywhere in our study area the seaward tip of the backstop must lie beneath the mixed vergence zone and the highest point in the wedge excepting the carbonate cap in the southern two profiles. Furthermore, landward of this tip, the roof of the backstop must be seaward dipping, because it deforms younger wedge sediments into the extended landward vergence zone that we observe toward the Sunda Trench [*Byrne and Hibbard*, 1987]. Velocity models generated for this part of the margin [*Chauhan et al*., 2009; *Klingelhoefer et al*., 2010; *Singh et al*., 2012; *Shulgin et al*., 2013; *Tang et al*., 2013] confirm that this backstop must also be composed of material with a compressional wave velocity in the ~5.5–6.8 km/s range, signifying a composition that approximates either continental crust or older, lithified accreted sediments overlying such crust.

Several studies have proposed backstop models offshore of northern Sumatra with varying results as different input data are used. Close to the deformation front, a backstop is inferred from gravity data suggesting higher sediment densities [*McNeill et al*., 2006; *McNeill and Henstock*, 2014]. From single-channel seismic profiles, a backstop is inferred using observed pattern of near-surface wedge deformation [*Fisher et al*., 2007; *Mosher et al*., 2008]. From deep-penetration seismic and tomography, a proposed backstop is extended to western edge of the Aceh Basin (Figure 6a) [*Chauhan et al*., 2009; *Singh et al*., 2012], based on a seaward dipping reflector in that location. A backstop under the Simeulue Basin (Figure 6c [*Klingelhoefer et al*., 2010]) and around Simeulue Island [*Shulgin et al*., 2013] is inferred based on seismic velocities of ~6–7 km/s. Numerical modeling, incorporating frictional properties of the sediment and associated mantle wedge by *Tan et al.* [2012], suggests that the overriding plate crust acts as a backstop, extending seaward toward the Sunda Trench. Using a compressional wave velocity model, *Tang et al.* [2013] proposed a backstop extending beyond Simeulue Island toward the trench. These diverse observations are essentially in agreement with our proposed backstop model.

While we propose a rigid, seaward dipping backstop within the inner wedge to be responsible for the observed zone of landward vergence, there is also a possibility of a dynamic backstop farther seaward [*Kopp and Kukowski*, 2003]. A dynamic backstop is defined as sediment accreted against a rigid backstop and characterized by increasing lithification of accreted material [*Kopp and Kukowski*, 2003]. *McNeill and Henstock* [2014] identify a density anomaly situated near the deformation front that they propose contributes to the slope break and relatively steep frontal slope (5–6°) of the outer wedge; this anomaly could represent such a dynamic backstop, located seaward of our proposed rigid backstop.

The composition of the backstop under the Aceh Basin and adjacent accretionary prism is still being debated. *Berglar et al.* [2008], based on seismic data and core samples down to 3 km depth within Simeulue Basin, have pointed out that their observed acoustic basement is likely pre-Neogene in age, composed either of a preexisting continental shelf [*Rose*, 1983] or fore-arc sediments deposited in Late Mesozoic-early Tertiary [*Karig et al*., 1979; *Rose*, 1983]. However, *Martin et al.* [2014] have concluded that the basement of the Aceh Basin

is Oligocene or younger. The Nicobar Fan, the presumed primary source of the sediment forming the accretionary prism, has been suggested to be no older than late Miocene-early Pliocene [*Curray and Moore*, 1971; *Bowles et al*., 1978]; *Curray and Moore* [1974] have suggested that the accretionary prism formed in the late Miocene. Conversely, velocity models by *Singh et al.* [2008] and *Chauhan et al.* [2009] suggest that Aceh Basin basement is crystalline and part of the Sunda Block, the same as that underlying the Simeulue Basin [*Klingelhoefer et al*., 2010; *Shulgin et al*., 2013]. Based on tectonic models, *Barber and Crow* [2003] have proposed that this continental block offshore of northern Sumatra is granite of Jurassic-Cretaceous age. If the estimated seaward extent of our backstop (Figure 5, green dashed line) is accurate, then this backstop may consist of an older sedimentary deposit or be of continental origin. Extant velocity models also support the hypothesis. Regardless, there is a large range among extant backstop age interpretations, and further investigation is required.

6.4. Implication for Tsunamigenic Earthquakes

How the structure of the Sumatra accretionary wedge links the 2004 great earthquake and its unusually large accompanying tsunami is still not well established. *Gulick et al.* [2011] and *Geersen et al.* [2013] have proposed that due to the thick and potentially indurated nature of incoming sediments, coseismic rupture propagated closer to the trench, enhancing tsunamigenic potential. Our study suggests that the wedge interior, containing a strong backstop inboard and possibly a dynamic backstop outboard, along with rapidly consolidating accreted sediment near the deformation front [*Gulick et al*., 2011], may together act as a rigid block coseismically. Effectively, such a model extends velocity-weakening rheology seaward, allowing for coseismic rupture closer to the Sunda Trench and thereby enhancing tsunamigenic potential.

7. Conclusions

Structural and morphology interpretations of the accretionary prism offshore of northern Sumatra, based on both seismic and bathymetric data, allow us to observe and infer features within the region of maximum slip for the 2004 Sumatran-Andaman great earthquake that may have a bearing on tsunamigenic potential. First, differences in strike between the deformation front and ridges within the plateau are suggested to be the result of slope failures occurring along the deformation front, which occur more extensively in the southern portion of the study area. Second, the existence of tilted sediments in piggyback basins suggests recent and continuing activity of flanking thrust faults; ongoing deformation/shortening of the shallow prism is indicated. Third, we observed three prominent structural zones, which are consistent along strike (Figure 5 and Table 2): (1) landward vergent folds closer to the Sunda Trench, (2) seaward vergent folds characterizing the eastern plateau toward the Aceh Basin, and (3) an intervening region of mixed vergent folds. Such an extended region of landward vergence is rarely observed in accretionary prisms around the world; we conclude that this zone suggests the existence of a seaward dipping backstop. Fourth, we can infer the likely geometry of such a backstop (Figure 6): (a) the seaward tip of this backstop lies under the bathymetrically shallowest portion of the wedge (Figure 5) and (b) the roof of the backstop under the Aceh Basin is along an acoustically strong reflector at a depth of ~6 s. This backstop may be composed of continental crust of the Sunda Block or an older, lithified and metamorphosed sedimentary block from a time of earlier accretion. We also allow for the possibility of a dynamic backstop located seaward of the rigid backstop, with a gradient of lithification increasing landward from the trench, to aid in explaining the slope and position of the outermost wedge front.

The existence of a strong inner wedge, based on its morphology and shallow structure, the presence of well-lithified sediment near the deformation front, and a consistent landward vergence zone inboard of the deformation front all suggest that the northern Sumatra wedge could act as a solid translatable block during an earthquake, allowing rupture energy to propagate toward the Sunda Trench. Other accretionary prisms that exhibit similar morphology, such as a wide fore-arc and landward vergence zone, occur in at least portions of the margin of Cascadia and southwest Alaska. We speculate that these margins are especially prone to shallow updip slip during major earthquakes and are thus prone to damaging tsunamis.

Acknowledgments

We would like to express our appreciation to T.J. Henstock, L.C. McNeill, K. Berglar, D. Franke, C. Goldfinger, J.R. Patton, T. Fujiwara, and the crew of the *HMS Scott* of the UK Royal Navy for providing MCS and multibeam bathymetry data used in this research and to K.M. Martin for processing the SUMUT MCS profiles. We thank Editor J. Geissman and Associate Editor J.B.H. Shyu, reviewer L.C. McNeill, and an anonymous reviewer for their constructive suggestions and valuable comments on this manuscript. This research has been primarily funded by NSF (OCE-0623165) to Gulick, Austin, and Bangs and the Consortium for Ocean Leadership (COL SA 12–13) to Frederik. This is University of Texas Institute for Geophysics contribution 2746.

References

Ammon, C. J., et al. (2005), Rupture process of the 2004 Sumatra-Andaman earthquake, *Science*, *308*, 1133–1139.

Banerjee, P., F. Pollitz, B. Nagarajan, and R. Burgmann (2007), Coseismic slip distributions of the 26 December 2004 Sumatra-Andaman and 28 March 2005 Nias earthquakes from GPS static offsets, *Bull. Seismol. Soc. Am.*, *97*, S86–S102.

Barber, A. J., and M. J. Crow (2003), An evaluation of plate tectonic models for the development of Sumatra, *Gondwana Res.*, *6*, 1–28.

Berglar, K., C. Gaedicke, R. Lutz, D. Franke, and Y. S. Djajadihardja (2008), Neogene subsidence and stratigraphy of the Simeulue forearc basin, northwest Sumatra, *Mar. Geol.*, *253*, 1–13.
Berglar, K., C. Gaedicke, D. Franke, S. Ladage, F. Klingelhoefer, and Y. S. Djajadihardja (2010), Structural evolution and strike-slip tectonics off north-western Sumatra, *Tectonophysics*, *480*, 119–132.
Bowles, F. A., W. F. Ruddiman, and W. H. Jahn (1978), Acoustic stratigraphy, structure, and depositional history of the Nicobar Fan, Eastern Indian Ocean, *Mar. Geol.*, *26*, 269–288.
Briggs, R. W., et al. (2006), Deformation and slip along the Sunda megathrust in the great 2005 Nias-Simeulue earthquake, *Science*, *311*, 1897–1901, doi:10.1126/science.1122602.
Brocher, T. M. (2005), Compressional and shear wave velocity versus depth in the San Francisco Bay Area, California: Rules for USGS Bay Area velocity.
Byrne, D. E., W.-H. Wang, and D. M. Davis (1993), Mechanical role of backstops in the growth of forearcs, *Tectonics*, *12*, 123–144, doi:10.1029/92TC00618.
Byrne, T., and J. Hibbard (1987), Landward vergence in accretionary prisms: The role of the backstop and thermal history, *Geology*, *15*(12), 1163.
Chauhan, A. P. S., S. C. Singh, N. D. Hananto, H. Carton, F. Klingelhoefer, J. X. Dessa, H. Permana, N. J. White, and D. Graindorge (2009), Seismic imaging of forearc backthrusts at northern Sumatra subduction zone, *Geophys. J. Int.*, *179*, 1772–1780.
Curray, J. R. (2005), Tectonics and history of the Andaman Sea region, *J. Asian Earth Sci.*, *25*(1), 187–232.
Curray, J. R., and D. G. Moore (1971), Growth of the Bengal deep-sea fan and denundation in the Himalayas, *Geol. Soc. Am. Bull.*, *82*, 563–572.
Curray, J. R., and D. G. Moore (1974), Sedimentary and tectonic processes in the Bengal deep-sea fan and geosyncline, in *The Geology of Continental Margins*, edited by C. A. Burk and C. L. Drake, pp. 617–627, Springer, New York.
Davis, D. M., J. Suppe, and F. A. Dahlen (1983), Mechanics of fold-and-thrust belts and accretionary wedges, *J. Geophys. Res.*, *88*, 1153–1172, doi:10.1029/JB088iB02p01153.
Dean, S. M., L. C. McNeill, T. J. Henstock, J. M. Bull, S. P. S. Gulick, J. A. Austin Jr., N. L. B. Bangs, Y. S. Djajadihardja, and H. Permana (2010), Contrasting décollement and prism properties over the Sumatra 2004–2005 earthquake rupture boundary, *Science*, *329*, 207–210.
Dorobek, S. L. (2008), Carbonate-platform facies in volcanic-arc settings: Characteristics and controls on deposition and stratigraphic development, *Geol. Soc. Am. Spec. Pap.*, *436*, 55–90.
Fisher, D., D. C. Mosher, J. A. Austin Jr., S. P. S. Gulick, T. Masterlark, and K. Moran (2007), Active deformation across the Sumatran forearc over the December 2004 M_w 9.2 rupture, *Geology*, *35*, 99.
Fujiwara, T., S. Kodaira, T. No, Y. Kaiho, N. Takahashi, and Y. Kaneda (2011), The 2011 Tohoku-Oki earthquake: Displacement reaching the trench axis, *Science*, *334*, 1240.
Geersen, J., L. McNeill, T. J. Henstock, and C. Gaedicke (2013), The 2004 Aceh-Andaman Earthquake: Early clay dehydration controls shallow seismic rupture, *Geochem. Geophys. Geosyst.*, *14*, 3315–3323, doi:10.1002/ggge.20193.
Geist, E. L., S. L. Bilek, D. Arcas, and V. Titov (2006), Differences in tsunami generation between the December 26, 2004 and March 28, 2005 Sumatra earthquakes, *Earth Planets Space*, *58*, 185–193.
Graindorge, D., et al. (2008), Impact of lower plate structure on upper plate deformation at the NW Sumatran convergent margin from seafloor morphology, *Earth Planet. Sci. Lett.*, *275*, 201–210.
Gulick, S. P. S., A. M. Meltzer, and S. H. Clarke (1998), Seismic structure of the southern Cascadia subduction zone and accretionary prism north of the Mendocino triple junction, *J. Geophys. Res.*, *103*, 27,207–27,222, doi:10.1029/98JB02526.
Gulick, S. P. S., J. A. J. Austin, L. C. McNeill, N. L. B. Bangs, K. M. Martin, T. J. Henstock, J. M. Bull, S. M. Dean, Y. S. Djajadihardja, and H. Permana (2011), Updip rupture of the 2004 Sumatra earthquake extended by thick indurated sediments, *Nat. Geosci.*, *4*, 453–456.
Gutscher, M.-A., N. Kukowski, J. Malavieille, and S. Lallemand (1998), Episodic imbricate thrusting and underthrusting: Analog experiments and mechanical analysis applied to the Alaskan accretionary wedge, *J. Geophys. Res.*, *103*, 10,161–10,176, doi:10.1029/97JB03541.
Gutscher, M.-A., D. Klaeschen, E. R. Flueh, J. Malavieille, and D. Kiel (2001), Non-Coulomb wedges, wrong-way thrusting, and natural hazards in Cascadia, *Geology*, *29*, 379–382.
Henstock, T. J., L. C. McNeill, and D. R. Tappin (2006), Seafloor morphology of the Sumatran subduction zone: Surface rupture during megathrust earthquakes?, *Geology*, *34*, 485.
Ishii, M., P. M. Shearer, H. Houston, and J. E. Vidale (2005), Extent, duration and speed of the 2004 Sumatra-Andaman earthquake imaged by the Hi-Net array, *Nature*, *435*, 933–936.
Karig, D. E. (1977), Growth pattern on the upper trench slope, in *Island Arcs, Deep Sea Trenches and Back-Arc Basins*, *Maurice Ewing Ser.*, vol. 1, pp. 175–185, AGU, Washington, D. C.
Karig, D. E., S. Suparka, G. F. Moore, and P. E. Hehanussa (1979), Structure and Cenozoic evolution of the Sunda arc in the central Sumatra region, *AAPG Mem.*, *29*, 1–15.
Klingelhoefer, F., M.-A. Gutscher, S. Ladage, J.-X. Dessa, D. Graindorge, D. Franke, C. André, H. Permana, T. Yudistira, and A. Chauhan (2010), Limits of the seismogenic zone in the epicentral region of the 26 December 2004 great Sumatra-Andaman earthquake: Results from seismic refraction and wide-angle reflection surveys and thermal modeling, *J. Geophys. Res.*, *115*, B01304, doi:10.1029/2009JB006569.
Kopp, H., and N. Kukowski (2003), Backstop geometry and accretionary mechanics of the Sunda margin, *Tectonics*, *22*(6), 1072, doi:10.1029/2002TC001420.
Kopp, H., et al. (2008), Lower slope morphology of the Sumatra trench system, *Basin Res.*, *20*, 519–529.
Lutz, R., C. Gaedicke, K. Berglar, S. Schloemer, D. Franke, and Y. S. Djajadihardja (2011), Petroleum systems of the Simeulue fore-arc basin, offshore Sumatra, Indonesia, *Am. Assoc. Pet. Geol. Bull.*, *95*, 1589–1616.
MacKay, M. E. (1995), Structural variation and landward vergence at the toe of the Oregon accretionary prism, *Tectonics*, *14*, 1309–1320, doi:10.1029/95TC02320.
MacKay, M. E., G. F. Moore, G. R. Cochrane, J. Casey Moore, and L. V. D. Kulm (1992), Landward vergence and oblique structural trends in the Oregon margin accretionary prism: Implications and effect on fluid flow, *Earth Planet. Sci. Lett.*, *109*, 477–491.
Malod, J.-A., et al. (1993), Déformations du bassin d'avant-arc au Nord-Ouest de Sumatra: Une réponse à la subduction oblique, *C. R. Acad. Sci.*, *316*(6), 791–797.
Martin, K. M., S. P. S. Gulick, J. A. Austin, K. Berglar, D. Franke, and Udrekh (2014), The West Andaman Fault: A complex strain-partitioning boundary at the seaward edge of the Aceh Basin, offshore Sumatra, *Tectonics*, *33*, 786–806, doi:10.1002/2013TC003475.
McNeill, L. C., and T. J. Henstock (2014), Forearc structure and morphology along the Sumatra-Andaman subduction zone, *Tectonics*, *33*, 112–134, doi:10.1002/2012TC003264.
McNeill, L. C., T. J. Henstock, D. R. Tappin, and J. R. Curray (2006), Forearc morphology and thrust vergence, Sunda subduction zone, *Eos Trans. AGU*, *87*(52), Fall Meet. Suppl., Abstract U44A-07.

Moeremans, R., S. C. Singh, M. Mukti, J. McArdle, and K. Johansen (2014), Seismic images of structural variations along the deformation front of the Andaman–Sumatra subduction zone: Implications for rupture propagation and tsunamigenesis, *Earth Planet. Sci. Lett.*, *386*, 75–85.
Molnar, P., and P. Tapponnier (1975), Cenozoic tectonic of Asia: Effects of a continental collision, *Science*, *189*(4201), 419–426.
Moore, C., and A. Allwardt (1980), Progressive deformation of a Tertiary Trench Slope, Kodiak Islands, Alaska, *J. Geophys. Res.*, *85*, 4741–4756, doi:10.1029/JB085iB09p04741.
Moran, K., J. A. J. Austin, and D. R. Tappin (2005), Survey presents broad approach to tsunami studies, *Eos Trans. AGU*, *86*, 430–431, doi:10.1029/2005EO440005.
Mosher, D. C., J. A. Austin Jr., D. Fisher, and S. P. S. Gulick (2008), Deformation of the northern Sumatra accretionary prism from high-resolution seismic reflection profiles and ROV observations, *Mar. Geol.*, *252*, 89–99.
Müller, R. D., M. Sdrolias, C. Gaina, and W. R. Roest (2008), Age, spreading rates, and spreading asymmetry of the world's ocean crust, *Geochem. Geophys. Geosyst.*, *9*, Q04006, doi:10.1029/2007GC001743.
Natawidjaja, D. H., K. Sieh, J. Galetzka, B. W. Suwargadi, H. Cheng, R. L. Edwards, and M. Chlieh (2007), Interseismic deformation above the Sunda megathrust recorded in coral microatolls of the Mentawai Islands, West Sumatra, *J. Geophys. Res.*, *112*, B02404, doi:10.1029/2006JB004450.
Pollitz, F. F., R. Bürgmann, and P. Banerjee (2011), Geodetic slip model of the 2011 *M*9.0 Tohoku earthquake, *Geophys. Res. Lett.*, *38*, L00G08, doi:10.1029/2011GL048632.
Prawirodirdjo, L., Y. Bock, J. F. Genrich, M. Green, and S. Sutisna (2000), One century of tectonic deformation along the Sumatran Fault from triangulation and Global Positioning System surveys, *J. Geophys. Res.*, *105*, 28,343–28,361, doi:10.1029/2000JB900150.
Reed, D. L., E. A. Silver, J. E. Tagudin, T. H. Shipley, and P. Vrolijk (1990), Relations between mud volcanoes, thrust deformation, slope sedimentation, and gas hydrate, offshore north Panama, *Mar. Pet. Geol.*, *7*, 44–54.
Rhie, J., D. Dreger, R. Burgmann, and B. Romanowicz (2007), Slip of the 2004 Sumatra–Andaman earthquake from joint inversion of long-period global seismic waveforms and GPS static offsets, *Bull. Seismol. Soc. Am.*, *97*, S115–S127.
Rose, R. (1983), Miocene carbonate rocks of Sibolga Basin, northwest Sumatra, in *Twelfth Annual Convention*, pp. 107–125, Indonesian Petroleum Association.
Sclater, J. G., and R. L. Fisher (1974), Evolution of the East: Central Indian Ocean, with emphasis on the tectonic setting of the Ninetyeast Ridge, *GSA Bull.*, *85*(5), 683–702.
Seely, D. R. (1977), The significance of landward and oblique structural trends on trench inner slopes, in *Island Arcs Deep Sea Trenches and Back-Arc Basins*, edited by M. Talwani and W. C. Pitman, pp. 187–198, AGU, Washington, D. C.
Shulgin, A., H. Kopp, D. Klaeschen, C. Papenberg, F. Tilmann, E. R. Flueh, D. Franke, U. Barckhausen, A. Krabbenhoeft, and Y. Djajadihardja (2013), Subduction system variability across the segment boundary of the 2004/2005 Sumatra megathrust earthquakes, *Earth Planet. Sci. Lett.*, *365*, 108–119.
Sibuet, J.-C., C. Rangin, X. Lepichon, S. C. Singh, A. Cattaneo, D. Graindorge, F. Klingelhoefer, J.-y. Lin, J. A. Malod, and T. Maury (2007), 26th December 2004 great Sumatra–Andaman earthquake: Co-seismic and post-seismic motions in northern Sumatra, *Earth Planet. Sci. Lett.*, *263*, 88–103.
Singh, S. C., et al. (2008), Seismic evidence for broken oceanic crust in the 2004 Sumatra earthquake epicentral region, *Nat. Geosci.*, *1*, 777–781.
Singh, S. C., H. Carton, A. S. Chauhan, S. Androvandi, A. Davaille, J. Dyment, M. Cannat, and N. D. Hananto (2011), Extremely thin crust in the Indian Ocean possibly resulting from plume-ridge interaction, *Geophys. J. Int.*, *184*(1), 29–42.
Singh, S. C., A. P. S. Chauhan, A. J. Calvert, N. D. Hananto, D. Ghosal, A. Rai, and H. Carton (2012), Seismic evidence of bending and unbending of subducting oceanic crust and the presence of mantle megathrust in the 2004 great Sumatra earthquake rupture zone, *Earth Planet. Sci. Lett.*, *321–322*, 166–176.
Smith, W. H. F., and P. Wessel (1990), Gridding with continuous curvature splines in tension, *Geophysics*, *55*, 293–305.
Storti, F., R. S. Marin, C. Faccenna, and A. C. Sainz (2001), Role of the backstop-to-cover thickness ratio on vergence partitioning in experimental thrust wedges, *Terra Nova*, *13*, 413–417.
Taira, A., et al. (1998), Nature and growth rate of the Northern Izu-Bonin (Ogasawara) arc crust and their implications for continental crust formation, *Isl. Arc*, *7*, 395–407.
Tan, E., L. L. Lavier, H. J. A. Van Avendonk, and A. Heuret (2012), The role of frictional strength on plate coupling at the subduction interface, *Geochem. Geophys. Geosyst.*, *13*, Q10006, doi:10.1029/2012GC004214.
Tang, G., et al. (2013), 3-D active source tomography around Simeulue Island offshore Sumatra: Thick crustal zone responsible for earthquake segment boundary, *Geophys. Res. Lett.*, *40*, 48–53, doi:10.1029/2012GL054148.
Wang, K., and Y. Hu (2006), Accretionary prisms in subduction earthquake cycles: The theory of dynamic Coulomb wedge, *J. Geophys. Res.*, *111*, B06410, doi:10.1029/2005JB004094.
Wang, W., and D. M. Davis (1996), Sandbox model simulation of forearc evolution and noncritical wedges, *J. Geophys. Res.*, *101*, 11,329–11,339, doi:10.1029/96JB00101.
Wessel, P., and W. H. F. Smith (1991), Free software helps map and display data, *Eos Trans. AGU*, *72*, 441–446, doi:10.1029/90EO00319.
Wessel, P., and W. H. F. Smith (1998), New, improved version of Generic Mapping Tools released, *Eos Trans. AGU*, *79*, 579, doi:10.1029/98EO00426.